CLM-P763

CLM-P763

UKAEA

Preprint

AN INTERPRETATION OF DISRUPTIONS IN TOKAMAK SIMULATIONS

J. W. EASTWOOD
W. ARTER

CULHAM LABORATORY
Abingdon, Oxfordshire

1985

CLM-P763

AN INTERPRETATION OF DISRUPTIONS IN TOKAMAK SIMULATIONS

James W Eastwood and Wayne Arter

Culham Laboratory, Abingdon, Oxon, OX14 3DB, England

(Euratom/UKAEA Fusion Association)

Abstract

The broad spectrum of explosively growing modes observed in multihelicity tearing mode simulations of tokamak plasmas can be accounted for by a nonphysical feedback mechanism. It is shown that spatially discretised magnetohydrodynamic (MHD) equations admit both attracting finite time singularities and exponential, but bounded, deviations from solutions of differential MHD. Finally, means of avoiding the nonphysical behaviour, which is characterised by poor energy conservation, are given.

PACS 52.30.+r 52.65.+z 52.55.-s

(Submitted for publication in Physical Review Letters)

November,1985

Experiment and theory indicate that tearing modes are intimately involved in disruptions. Explanations in terms of MHD activity which have been put forward fall into three categories: i) thermal shorting, where conditions in the tokamak slowly change until large magnetic islands of different helicity overlap each other and the wall[1], ii) radiation catastrophe, where a radiation front propagates in from the wall, narrowing the current channel and leading to MHD instability[2] and iii) destabilisation due to nonlinear MHD effects [3,4]. Case i) is most relevant to "low-q" disruptions, case ii) to "density limit" disruption. We consider here only case (iii).

In case iii), it is assumed that unspecified mechanisms lead to current profiles which are unstable to low poloidal (m) and toroidal (n) wavenumber tearing modes; typically m/n are 2/1 and 3/2. These modes interact to destabilise others on a rapid timescale, leading to a broad spectrum of explosively growing modes. In the so called "hard disruption" cases, numerical models are unable to compute through the explosive growth phase but it is believed that the resulting ergodic field would lead to heat loss and current collapse. We demonstrate here that the explosive phase observed in numerical simulations before termination can be accounted for by a nonphysical feedback mechanism. Our results indicate the conditions which are required for broadband mode growth and so show how to avoid these 'disruptions'.

The feedback mechanism is simply a manifestation of insufficient spatial resolution. In an almost ideal plasma, nonlinear coupling cascades energy to shorter wavelengths. If dissipation is sufficiently weak, energy can flow to wavelengths unresolved by the radial grid. These subgrid scale components masquerade as (or 'alias') longer wavelengths on the mesh[5]. If aliases have the correct phases, their contributions to mesh resolved wavelengths can enhance the nonlinear terms which cause them, so leading to positive feedback destabilisation.

Figure 1 gives a simple pictorial representation of the alias coupling mechanism. Quadratic nonlinearities cause the wavelength of three mesh spacings ($\lambda = 3H$) to generate a component with $\lambda = 3H/2$. When sampled on the mesh, both of these components appear as contributions to the component $\lambda = 3H$. With the phases shown, the alias contribution ($\lambda =$

3H/2) enhances the amplitude of the principal component ($\lambda = 3H$). A larger principal component leads to a larger alias, and so forth, leading to explosive growth. More generally, alias coupling will involve many wavelengths with the result that many modes will grow. Such behaviour may look superficially like a physical process.

To illustrate our interpretation, we consider the reduced MHD equations[6], which comprise evolutionary equations for toroidal vorticity, ω and poloidal magnetic flux, ϕ:-

$$\dot{\omega} + \underset{\sim}{v}.\underset{\sim}{\nabla}\omega = \underset{\sim}{B}.\underset{\sim}{\nabla}j + \nu\nabla_\perp^2\omega \quad , \tag{1}$$

$$\dot{\phi} + \underset{\sim}{v}.\underset{\sim}{\nabla}\phi = \frac{\partial\phi}{\partial z} + \eta\nabla_\perp^2\phi \quad , \tag{2}$$

where

$$\underset{\sim}{v} = \underset{\sim}{\nabla}\phi \times \underset{\sim}{e}_z \quad ; \quad \underset{\sim}{B} = \underset{\sim}{\nabla}\psi \times \underset{\sim}{e}_z + \underset{\sim}{e}_z \; ; \tag{3}$$

$$\nabla_\perp^2\phi = -\omega \quad ; \quad \nabla_\perp^2\psi = -j \quad ; \tag{4}$$
$$\nabla_\perp^2 \equiv \nabla^2 - \partial^2/\partial z^2 \; .$$

$\underset{\sim}{e}_z$ is the unit vector in the toroidal (z) direction. $\underset{\sim}{v}$, $\underset{\sim}{B}$, ϕ, j, η and ν are respectively flow velocity, magnetic field, stream function, toroidal current density, resistivity and viscosity. These equations have the energy conservation law

$$\frac{d}{dt}\int_v d\tau\left(\left|\underset{\sim}{\nabla}\phi\right|^2 + \left|\underset{\sim}{\nabla}\psi\right|^2\right)/2 - \int_s \psi\underset{\sim}{\nabla}\psi.d\underset{\sim}{\sigma} + \int_v (\eta j^2 + \nu\omega^2)d\tau = 0 \tag{5}$$

for a volume v bounded by surface s through which there is no net kinetic energy flux.

Computer simulations of these equations usually employ finite differences in radius and spectral approximations in poloidal and toroidal angles. We locally model them using cartesians (x,y,z), where we treat x as the radial, y as the poloidal and z as the toroidal coordinate. Since our mechanism does not rely on external driving terms or gradients in z, we assume uniformity in z and periodicity in x and y. The semidiscrete approximations to Eqs.(1) - (4) are obtained by replacing derivatives with respect to x by finite differences, functional dependences on y by truncated fourier series, and then projecting the resulting expressions onto a set of mesh points (in x) and fourier modes (in y). If we write Eqs.(1) - (4) symbolically as $\dot{u} - F(u) = 0$, then the finite difference, truncated mode expression becomes $\dot{\tilde{u}} - \tilde{F} = \varepsilon$, and the projection gives

$$\int_0^{L_x} dx\ \delta(x-x_p) \int_0^{L_y} dy\ e^{-i\frac{2\pi\ell y}{L}} (\dot{\tilde{u}} - \tilde{F}) = 0 \qquad (6)$$

where (L_x,L_y) are the (x,y) period lengths, x_p $(p\ \varepsilon[0,N_x-1])$ is the position of mesh point p and ℓ is the y-wavenumber. Taking a uniform mesh in x, $x_p = pH = pL_x/N_x$ allows the x coordinate to be fourier transformed to give the k-space representation of the semidiscrete equations:-

$$\kappa_\perp^2 \dot{\tilde{\phi}} = - \underset{\sim}{e}_z \cdot [\ \underset{\sim}{K}\tilde{\phi} \otimes \underset{\sim}{K}\ \kappa_\perp^2\ \tilde{\phi} - \underset{\sim}{K}\tilde{\psi} \otimes \underset{\sim}{K}\ \kappa_\perp^2\ \tilde{\psi}] - \nu\ \kappa_\perp^4\ \tilde{\phi}\ , \qquad (7)$$

$$\dot{\tilde{\psi}} = \underset{\sim}{e}_z \cdot [\ \underset{\sim}{K}\ \tilde{\phi} \otimes \underset{\sim}{K}\ \tilde{\psi}\ ] - \eta\ \kappa_\perp^2\ \tilde{\psi}\ . \qquad (8)$$

The compact notation employed in Eqs.(7) and (8) is as follows: The transform pair for both x and y coordinates is given by

$$a(x) = \sum_{k=-K_o}^{K_o} \tilde{a}_k\ e^{i\frac{2\pi kx}{L}}\ ;\quad \tilde{a}_k = \frac{1}{L}\int_0^L a(x)\ e^{-i\frac{2\pi kx}{L}}\ dx\ ,$$

where $L = L_x$ or L_y, harmonics are zero for $|k| > K_o, K_o = (N-1)/2$ for N

odd and $K_o = N/2$ for N even and $N(= N_x$ or $N_y)$ is the number of mesh values or harmonics. $i\underset{\sim}{K}$ and $-\kappa_\perp^2$ are respectively transforms of the discrete approximations to $\underset{\sim}{\nabla}$ and $\nabla_\perp^2$. The symbol $\otimes$ denotes a convolution and cross product:-

$$\underset{\sim}{\tilde{f}} \otimes \underset{\sim}{\tilde{g}} \equiv \sum_{k',\ell'} \underset{\sim}{\tilde{f}}_{k',\ell'} \times \underset{\sim}{\tilde{g}}_{k-k',\ell-\ell'} . \qquad (9)$$

Implicit in Eqs.(7) and (8) is a sum over the aliases, n, introduced by sampling in x. Each term is a function of $(k + nN_x, \ell)$. The alias sum[5] periodically extends linear functions of k and periodically wraps round sums over k' in expressions like Eq.(9). For $|k| \leqslant K_o$, the only linear terms altered by aliasing are those for which $|k| = K_o$.

Simulation programs numerically integrate thousands of simultaneous ordinary differential equations (odes) of the form of Eqs.(7) and (8). We seek intrinsic properties of such systems by investigating solutions with particular spatial periodicities. The simplest nontrivial instances we have found are for $\tilde{\phi}$ odd and $\tilde{\psi}$ even in both indices k and ℓ, a spatial periodicity of 3 mesh points in the x direction ($-1 \leqslant k \leqslant 1$) and 5 wavenumbers ($-2 \leqslant \ell \leqslant 2$) in the y direction. This reduces Eq.(8) to the five odes:-

$$\dot{a} = -\eta a - 4dg - 2bf \quad \underline{- 4cf - 8eg} ,$$

$$\dot{b} = -\eta b + 2cg - 2ef + 2af ,$$

$$\dot{c} = -2\eta c - bg - 2df \quad \underline{- 3cg - 3ef - af} ,$$

$$\dot{d} = -4\eta d + 4ag + 4cf , \qquad (10)$$

$$\dot{e} = -5\eta e + bf \quad \underline{- 2ag} ,$$

and Eq.(7) to the two odes

$$2\dot{f} = -4\nu f - 4be - 4cd \quad \underline{+ 9fg + 9ec + ac} \ ,$$

$$5\dot{g} = -25\nu g + bc - 6ad \quad \underline{+ 8ae} \ ,$$

where we have taken $L_x = L_y = 2\pi$ and have ignored the smoothing effect of differencing, ie, $\underset{\sim}{K} = (k,\ell)$ and $\kappa_\perp^2 = k^2 + \ell^2$. Including smoothing changes numerical factors but not the nature of the solutions. a,...,g denote respectively $\tilde{\psi}_{1,0}$, $\tilde{\psi}_{0,1}$, $\tilde{\psi}_{1,1}$, $\tilde{\psi}_{0,2}$, $\tilde{\psi}_{1,2}$, $\tilde{\phi}_{1,1}$ and $\tilde{\phi}_{1,2}$. Forming the rate of change of specific total (magnetic + kinetic) energy, $\dot{E}$, by multiplying Eq.(7) by $\tilde{\phi}^*$ and (8) by $\kappa_\perp^2\tilde{\psi}^*$ and summing gives for the above 7th order model:-

$$\begin{aligned}\dot{E} = &-\eta(2a^2 + 2b^2 + 16c^2 + 32d^2 + 100e^2) \\ &-\nu(16f^2 + 100g^2) \\ &\underline{-12acf - 24aeg - 24c^2g + 12cef + 36f^2g} \ .\end{aligned} \qquad (11)$$

The underlined terms in Eqs.(10) and (11) are due to aliasing.

We identify three classes of solution of Eqs.(7) and (8); i) physical, ii) bounded with (typically exponential) excursions and iii) singular. Alias terms are necessarily small for physical solutions to occur. Setting alias terms in Eq.(11) to zero shows that in the limit of vanishing aliases, E is a uniformly decreasing function of time. The physical interpretation is that the undriven dissipative system eventually comes to rest due to resistivity and viscosity. It is also a statement of energy conservation; upon integration, the alias free form of Eq.(11) states that the sum of magnetic and kinetic energy and time integrated joule and viscous power is a constant, cf. Eq.(5).

A simple instance of Eq.(10) with bounded excursions in the phase space spanned by a,...g is that for initial conditions of zero magnetic field: $a = b = c = d = e = 0$ at $t = 0$. This yields

$$f = f_o \exp\{-2\nu t - 9 g_o[\exp(-5\nu t)-1]/10\nu\},$$

$$\dot{E} = -\nu(16f^2 + 100g^2) \underline{+ 36f^2 g} ,$$

where f_o and g_o are initial values of f and g. For $9g_o > 4\nu$ and small t, f will grow exponentially. Ultimately, f reaches a maximum $f_{max} \alpha f_o(g_o/\nu)^{-2/5}\exp(9g_o/10\nu)$. ie, linear increments of g_o lead to exponential increases of f_{max}. Setting $\nu = 0$ recovers the well known instance of exponential failure of incompressible fluid calculations[7].

Equation (10) [and also Eqs.(7) and (8)] may be written $\dot{x}_i = \alpha_{ijk} x_j x_k$ in the limit of small dissipation. This set of equations admits solutions with finite time singularities, $x_i = X_i/(t_o - t)$; $t_o > 0$, provided a) that real non-zero X_i can be found to satisfy $X_i = \alpha_{ijk} X_j X_k$ and b) that such solutions have finite domains of attraction for $t_o > 0$. Energy conservation shows the non-existence of nonzero real $\{X_i\}$ in the absence of aliases. Counterexamples can be found when alias terms are present; initial conditions $a = d = e = f = 0$ in Eq.(10) give for large (b,c,g)

$$(b,c,g) = (b_o,c_o,g_o)/(t_o - t)$$

where

$$(b_o,c_o,g_o) = (\pm\sqrt{10}, \mp\sqrt{10}, 1)/2 \text{ or } (\pm 2\sqrt{10}, \mp\sqrt{10}, 2)/2 .$$

Linear analysis shows that, for the first pair of coefficients, asymptotic solutions are stable to small perturbations for $t < t_o$, demonstrating the existence of attracting finite time singularities in the semidiscrete MHD equations. For small initial (b,c,g), the solutions exponentially decay.

Numerical solution of the set of Eqs.(10) for arbitrary initial conditions generates further particular solutions which fall into the three classes described. Singular solutions take the appearance of broadband mode growth as harmonics tend to their asymptotic values, growing as $1/(t_o - t)$. Similar behaviour is found using our three

dimensional spectral/finite difference code, FORBAK. This code differs from that of Ref.3 in that it has $\nu \neq o$ as an option, a different time integration scheme and timestep control, additional diagnostics and programmed current boundary conditions.

Figure 2 shows plots of island widths versus time for a calculation with $\nu = 0$, $S = 10^6 (= V_A a/\eta_o$ where V_A is the Alfven velocity, a is minor radius and η_o is resistivity at $r = 0$), an initial safety factor profile $q = q_o\left(1 + (r/r_o)^{2\lambda}\right)^{1/\lambda}$, $r_o = .567a$, $\lambda = 3.24$ and $q_o = 1.34$, $\eta(r) \alpha 1/j(r,t = o)$. The initial axisymmetric equilibrium was perturbed by 2/1 and 3/2 helical structures with island widths of .05a. The calculation used 100 radial grid points and 11 modes with helicities 0/0, 1/0, 1/1, 2/1, 3/2, 5/3 and 7/4.

The calculation terminated at time $t_o \approx .0016\ \tau_R$ because the linear stability criterion caused the timestep to become vanishingly small. Figure 3 gives log (energy) versus $-\log\left[(t_o - t)/\tau_R\right]$ for the case shown in figure 2. The slope 2 line shows that the calculation terminates with energy $\alpha\ (t_o - t)^{-2}$, ie, there is a $(t_o - t)^{-1}$ finite time singularity. Corresponding plots for mode kinetic and magnetic energies have the same $(t_o - t)^{-2}$ behaviour. Simulations using over 100 helical modes have shown similar behaviour. Radial sampling is the source of the aliases, so increasing the number of modes does not qualitatively change the feedback. To ensure nonlinear stability, orders of magnitude more radial mesh points would be required for the chosen S and ν values (c.f. below).

Analysis of model problems, such as Eq.(10), and physical argument show how the alias instability can be avoided. One approach is to prevent the energy cascade to subgrid scalelengths. Energy flows to shorter wavelengths due to nonlinear waves from transients, and from steepening gradients (as for instance in tangential discontinuities). The shortest scale lengths reached are determined by the balance between advective τ_a and diffusive timescales, τ_d. To prevent energy flow to length scales less than the grid spacing, H, we require $\tau_d/\tau_a < 0(1)$ at scale length H.

For Alfven wave processes, this implies a mesh Lundquist number, $L_u = HV_A/(\eta + \nu) < 0(1)$, and for flows, the mesh Reynolds number, R_e, and mesh magnetic Reynolds number, R_m, must also be small: $R_e = HV/\nu < 0(1)$, $R_m = HV/\eta < 0(1)$. V_A and V are measures of variations (eg, root mean square deviations) of Alfven and flow speeds. Satisfying these conditions causes solutions of Eq.(10) to have the property $\dot{E} < 0$, as may be deduced from Eq.(11). Increasing ν and η for the case illustrated in Fig.2 eliminates the singular behaviour and ultimately leads to good energy conservation: under such conditions, the final outcome of the simulation is saturated overlapping islands covering approximately half the plasma column[8] (whereupon, neglected physical processes affecting heat and particle confinement will become important).

Suppressing nonlinear instabilities by increasing viscosity and resistivity and/or reducing H has the drawback that Lundquist numbers, etc., accessible to computation are considerably smaller than those achieved in experiments. A more satisfactory approach is to devise discrete equations which guarantee bounded results. In ref. 9, it is shown that one such scheme, the EPIC scheme of Eastwood and Arter, outperforms state-of-the-art finite difference schemes, giving optimally accurate results.

This letter highlights the perils of ignoring the limitations of numerical simulations. Analytic and numerical integration of systems with spatial periodicity, and the outcome of tokamak simulations show the same singular behaviour that may be understood in terms of alias feedback instability. Our results do not preclude the existence of physical mechanisms with similar consequences to alias coupling, but they do suggest there is as yet no compelling evidence for such a mechanism from tokamak simulations. In the limits of large S and small ν/η appropriate to experimental conditions, simulations to evaluate the importance of factors such as cross section shaping, toroidal coupling, field programming, etc., may become very misleading when sharp gradients or alfven wave transients occur.

References

1
M.F. Turner and J.A. Wesson, Nucl. Fusion 22, 1069 (1982).

2
D.E.T.F. Ashby and M.H. Hughes, Nucl. Fusion 21, 911 (1981).

3
B.A. Carreras, H.R. Hicks, J.A. Holmes, B.V. Waddell, Phys. Fluids 23, 1811 (1980).

4
R. Izzo et al., Phys. Fluids 26, 2240 (1983).

5
R.W. Hockney and J.W. Eastwood, Computer Simulation Using Particles, (McGraw-Hill, New York, 1981).

6
H.R. Strauss, Phys. Fluids 19, 134 (1976).

7
N.A. Phillips, in The Atmosphere and Sea in Motion, ed. B. Bolin, (Rockefeller Institute Press, New York, 1959) p.501.

8
J.W. Eastwood and W. Arter, Culham Laboratory preprint CLM-P735, submitted to Phys. Fluids (1985).

9
J.W. Eastwood and W. Arter, in Numerical Methods for Fluid Dynamics, ed. K.W. Morton and M.J. Baines, (O.U.P., Oxford, 1985).

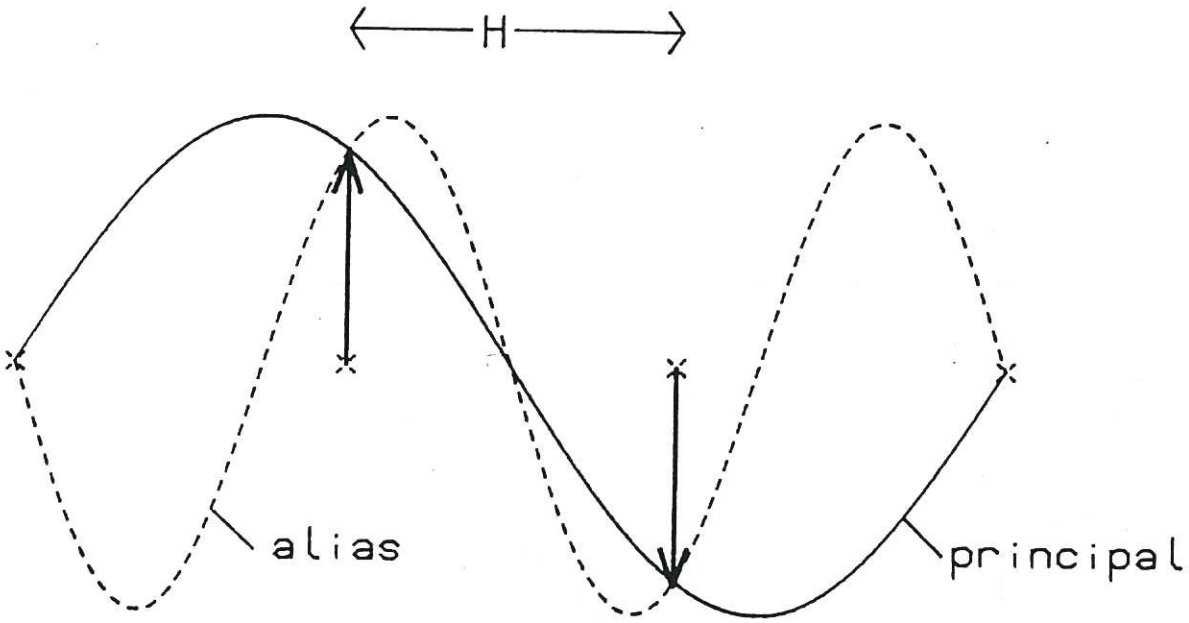

Fig. 1 Quadratic nonlinearities cause wavelengths $\lambda_0 = 3H$ to generate a component with $\lambda_1 = 3H/2$. When sampled on the mesh (crosses), these both contribute (shown by arrows) to mesh resolved wavelength 3H.

CLM-P763

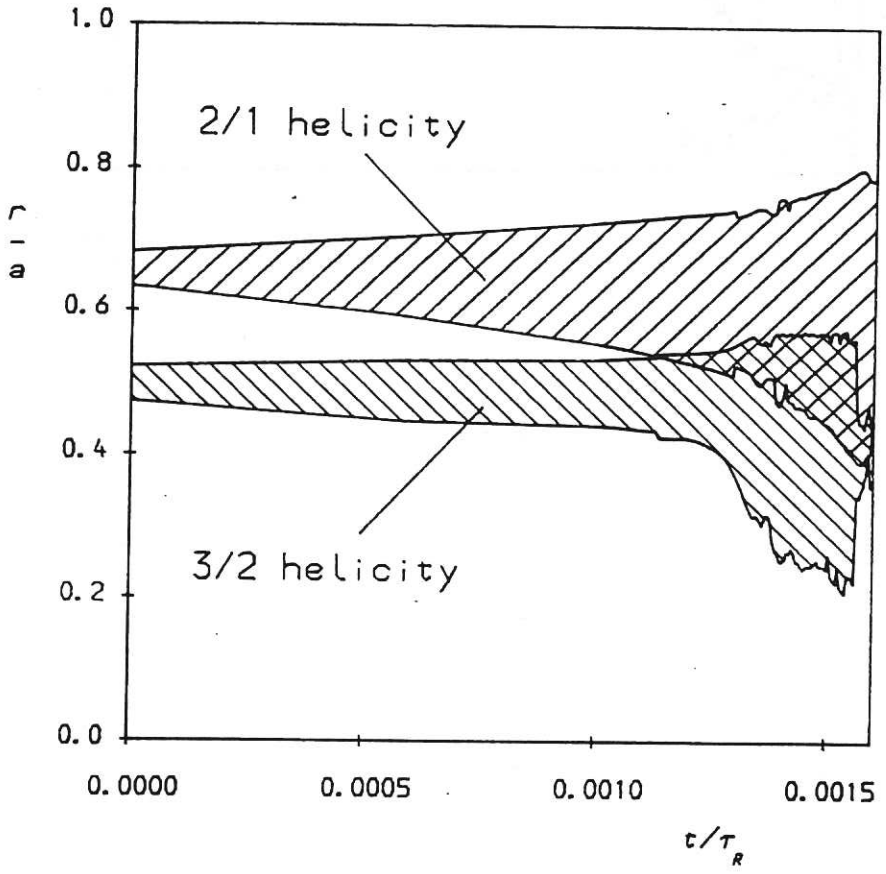

Fig. 2 Time dependence of the radial extent of magnetic islands for helicities 2/1 and 3/2. a is the minor radius and $\tau_R = a^2/\eta_0$. Island widths are defined as in ref. 3.

CLM-P763

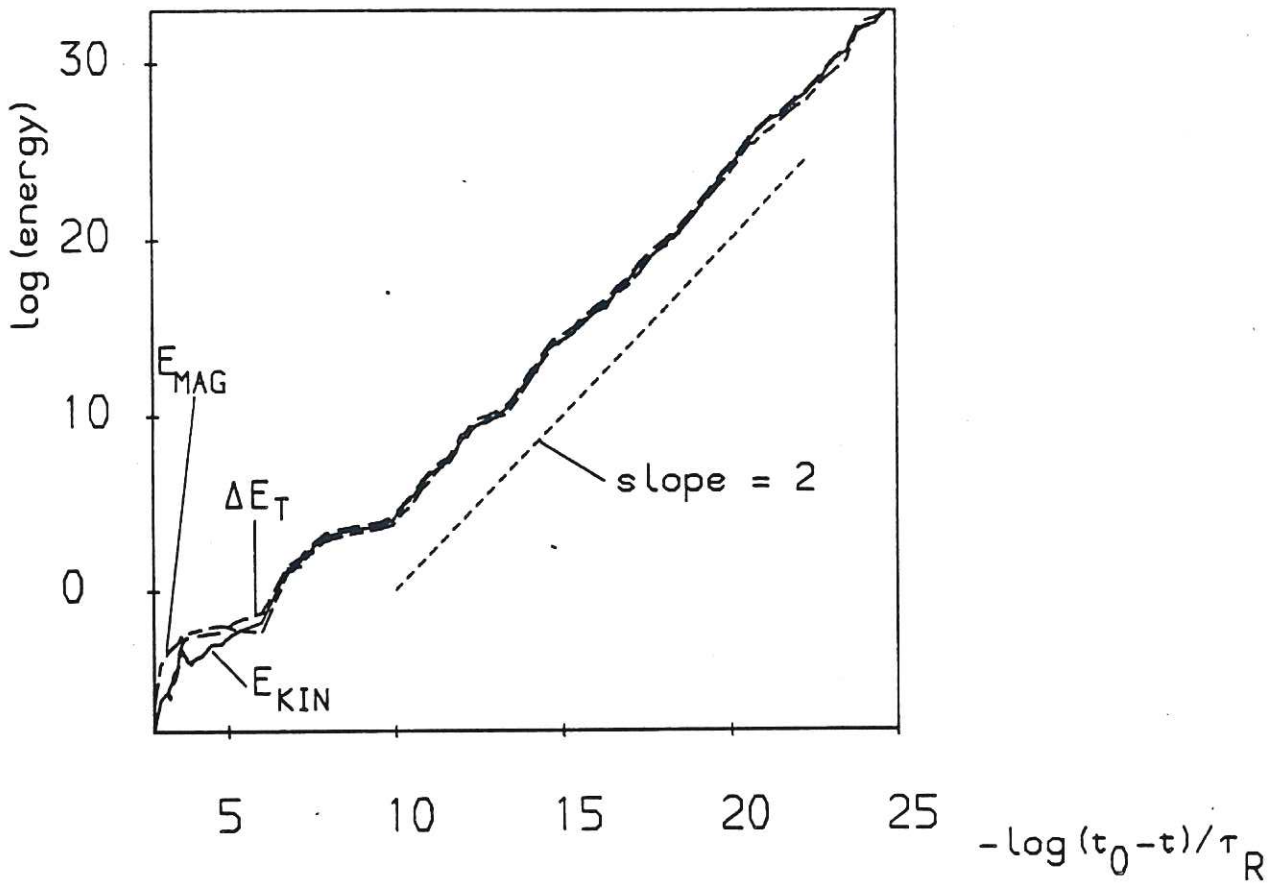

Fig. 3 Total magnetic, E_{MAG}, kinetic, E_{KIN}, and deviation from total energy conservation, ΔE_T plotted as a function of time $(t_0 - t)/\tau_R$.

CLM-P763